LINEAR MICROBUNCHING GAIN ESTIMATION INCLUDING CSR AND LSC IMPEDANCES IN RECIRCULATION MACHINES*

C. -Y. Tsai#, Virginia Tech, Blacksburg, VA 24061, USA
D. Douglas, R. Li, and C. Tennant, Jefferson Lab, Newport News, VA 23606, USA

Abstract

It is known that microbunching instability (MBI) has been one of the most challenging issues with the design of magnetic compressor chicanes for FEL or linear colliders, as well as the transport lines for recirculating or energy recovery linac machines. To more accurately quantify MBI in a single-pass or few-passes system and for more complete analyses, we extend our previously developed linear Vlasov solver [1, 2] to incorporate more relevant impedance models, including transient and steady-state coherent synchrotron radiation (CSR) and longitudinal space charge (LSC) impedances. Then the linearized Vlasov equation is numerically solved for the microbunching gain amplification factor. With application of this code to two specially designed transport arcs and a circulator cooling ring design of MEIC at Jefferson Lab, the resultant gain functions and spectra are presented and some results are compared with particle tracking simulation. We also discuss some underlying physics with inclusion of these collective effects. It is anticipated this more complete analysis can further improve the understanding of the MBI mechanisms and shed light on how to suppress or compensate MBI effects in such lattice designs.

INTRODUCTION

The beam quality preservation is of a general concern in delivering a high-brightness beam through a transport line or recirculation arc in the design of modern accelerators. Microbunching instability (MBI) has been one of the most challenging issues associated with such beamline designs. Any source of beam performance limitations in such recirculation or transport arcs must be carefully examined in order to preserve the beam quality, such as the coherent synchrotron radiation (CSR), longitudinal space-charge (LSC) and/or other high-frequency impedances that can drive microbunching instabilities.

To accurately quantify the direct consequence of microbunching effect, i.e. the gain amplification factor G (which shall be defined later), we further extend our previously developed semi-analytical simulation code [1, 2] to include more relevant impedance models, including both CSR and LSC impedances. The LSC effect stems from (upstream) non-uniformity of an electron beam and can accumulate an amount of energy modulation when a beam traverses a long section of a beamline. Such energy modulation can then convert to density modulation via momentum compaction R_{56} downstream the beamline. In addition, along the beamline, CSR due to electron radiation emission out of bending dipoles can have a significant effect on further amplifying such density to energy modulation. The accumulation and conversion between density and energy modulations can possibly cause serious microbunching gain amplification (or, microbunching instability).

In this paper, we would first summarize the impedance models used in our semi-analytical simulations. Then, we briefly introduce the methods of microbunching gain calculation: a kinetic model based on (linearized) Vlasov equation [3, 4], including direct and iterative approaches, and particle tracking by ELEGANT [5, 6]. In the same section, we devise a method to quantify the contribution of microbunching gains from individual stages based on the concept proposed in Ref. [4]. After that, we illustrate the calculated gain functions and spectra for our example lattices, including two comparative high-energy transport arcs and a circulator cooling ring (CCR) design for Medium-energy Electron Ion Collider (MEIC) project at Jefferson Lab [7]. Finally we discuss the underlying physics and summarize our observations from the simulation results. We hope this further accurate and complete consideration of microbunching gain estimation can be compared with currently experimental investigation [8, 9] and help shed light on how to further improve future lattice designs.

IMPEDANCE MODELS

For a (ultra-)relativistic electron beam traversing an individual dipole, CSR can have both steady-state and transient effects. In addition, when a beam goes through a long transport line, LSC can also have a significant effect on accumulating energy modulations. Here we quote the resultant analytical expressions for CSR and LSC impedances without further derivation:

Free-space Steady-state Non-ultrarelativistic CSR Impedance

For a relativistic electron beam ($\beta = 1$, $\gamma < \infty$) traversing a bending dipole, the free-space steady-state CSR impedance per unit length can be expressed as [10]:

$$\mathrm{Re}\left[Z_{CSR}^{s.s.NUR}(k(s);s)\right] = \frac{-2\pi k(s)^{1/3}}{|\rho(s)|^{2/3}}\mathrm{Ai}'\left(\frac{(k(s)|\rho(s)|)^{2/3}}{\gamma^2}\right) + \frac{k(s)\pi}{\gamma^2}\left(\int_0^{(k(s)|\rho(s)|)^{2/3}/\gamma^2}\mathrm{Ai}(\varsigma)\,d\varsigma - \frac{1}{3}\right) \quad (1)$$

$$\mathrm{Im}[Z_{CSR}^{s.s.NUR}(k(s);s)] \simeq \frac{2\pi k(s)^{1/3}}{|\rho(s)|^{2/3}}\left\{\frac{1}{3}\mathrm{Bi}'(x) + \int_0^x \begin{bmatrix}\mathrm{Ai}'(x)\mathrm{Bi}(t)\\ -\mathrm{Ai}(t)\mathrm{Bi}'(x)\end{bmatrix} dt\right\}$$

* This material is based upon work supported by the U.S. Department of Energy, Office of Science, Office of Nuclear Physics under contract DE-AC05-06OR23177.
#jcytsai@vt.edu

ISBN 978-3-95450-183-0

where $x=\left(k(s)|\rho(s)|\right)^{2/3}/\gamma^2$, $k = 2\pi/\lambda$ is the modulation wave number, $\rho(s)$ is the bending radius, and Ai and Bi are Airy functions. Under ultrarelativistic approximation ($\gamma\to\infty$), Eq. (1) is reduced to the well-known expression [11, 12]:

$$Z_{CSR}^{s.s.UR}(k(s);s)=\frac{-ik(s)^{1/3}A}{|\rho(s)|^{2/3}} \quad (2)$$

where the constant $A=-2\pi\left[\mathrm{Bi}'(0)/3+i\mathrm{Ai}'(0)\right]$.

Entrance Transient CSR Impedance

Prior to reaching steady-state interaction, the beam entering a bend from a straight section would experience the so-called entrance transient state, where the impedance per unit length can be obtained by Laplace transformation of the corresponding wakefield [13, 14, 15]:

$$Z_{CSR}^{ent}(k(s);s)=\frac{-4}{s^*}e^{-4i\mu(s)}+\frac{4}{3s^*}(i\mu(s))^{1/3}\Gamma\left(\frac{-1}{3},i\mu(s)\right) \quad (3)$$

where $\mu(s)=k(s)z_L(s)$, s^* is the longitudinal coordinate measured from dipole entrance, $z_L=\left(s^*\right)^3/24\rho^2$, and Γ is the upper incomplete Gamma function.

Exit Transient CSR Impedance

There are also exit CSR transient effects as a beam exits from a dipole. For the case with fields generated from an upstream electron (at retarded time) propagating across the dipole to downstream straight section, i.e. Case C of Ref. [15], the corresponding impedance per unit length can be similarly obtained by Laplace transformation:

$$Z_{CSR}^{exit}(k(s);s)=\frac{-4}{L_b+2s^*}e^{\frac{-ik(s)L_b^2}{6|\rho(s)|^2}\left(L_b+3s^*\right)} \quad (4)$$

where s^* is the longitudinal coordinate measured from dipole exit and L_b is the dipole length.

For the impedance expression with the case of fields generated from an electron (at retarded time) within a dipole propagating downstream the straight section, we use the following expression for the exit transient impedance [16]:

$$Z_{CSR}^{drif}(k(s);s)\approx\begin{cases}\frac{2}{s^*}, & \text{if } \rho^{2/3}\lambda^{1/3}\le s^*\le\lambda\gamma^2/2\pi\\ \frac{2k(s)}{\gamma^2}, & \text{if } s^*\ge\lambda\gamma^2/2\pi\\ 0, & \text{if } s^*<\rho^{2/3}\lambda^{1/3}\end{cases} \quad (5)$$

where s^* is the longitudinal coordinate measured from dipole exit. This expression assumes the exit impedance comes primarily from coherent edge radiation in the near-field region (i.e. $z < \lambda\gamma^2$), and in our simulation we only include transient effects [Eq. (4) and (5)] right after a nearby upstream bend. Here we note that these CSR models are valid only when the wall shielding effect is negligible. The wall shielding effect becomes important when the distance from the beam orbit to the walls h is to satisfy $h\le\left(\rho\lambda^2\right)^{1/3}$.

Longitudinal Space Charge Impedances [17]

Below we present two slightly different LSC impedance expressions implemented in our code. The first one is on-axis model, which assumes a transversely uniform density with circular cross section of radius r_b,

$$Z_{LSC}^{on-axis}(k(s);s)=\frac{4i}{\gamma r_b(s)}\frac{1-\xi K_1(\xi)}{\xi} \quad (6)$$

where $\xi=\frac{k(s)r_b(s)}{\gamma}$ and the transverse beam sizes can be obtained by the fitted result $r_b(s)\approx\frac{1.747}{2}\left(\sigma_x(s)+\sigma_y(s)\right)$ [18].

The second LSC model is the average model, which integrates the radial dependence [17,19],

$$Z_{LSC}^{ave}(k(s);s)=\frac{4i}{\gamma r_b(s)}\frac{1-2I_1(\xi)K_1(\xi)}{\xi} \quad (7)$$

where ξ is defined above the same way.

NUMERICAL METHODS

To quantify the MBI in a transport or recirculation arc, we estimate the microbunching amplification factor G (or, bunching factor) by two distinct methods. The first one, based on a kinetic model, is to solve a (linearized) Vlasov equation [3,4] using given impedance models [e.g. Eqs. (1-7)]. This method is of our primary focus in this paper. The second one, served as a benchmarking of the first method, is based on particle tracking (here we use ELEGANT [5,6]). For the former, after mathematical simplification of the linearized Vlsaov equation, we actually solve a general form of Volterra integral equation [3,4] in terms of the bunching factor. In our semi-analytical code, to facilitate us in simulating ERL-based lattices which usually contain spreaders/recombiners, we extend the existing formulation [3,4] to include both transverse horizontal and vertical bends. Below summarizes the governing equation for bunching factor g_k,

$$g_k(s)=g_k^{(0)}(s)+\int_0^s K(s,s')g_k(s')ds' \quad (8)$$

where the kernel function can be particularly expressed as

$$K(s,s')=\frac{ik}{\gamma}\frac{I(s)}{I_A}C(s')R_{56}(s'\to s)Z\left(kC(s'),s'\right)\times[\text{Landau damping}] \quad (9)$$

for the [Landau damping] term

$$[\text{Landau damping}]=\exp\left\{\frac{-k^2}{2}\left[\begin{array}{l}\varepsilon_{x0}\left(\beta_{x0}R_{51}^2(s,s')+\frac{R_{52}^2(s,s')}{\beta_{x0}}\right)\\ +\varepsilon_{y0}\left(\beta_{y0}R_{53}^2(s,s')+\frac{R_{54}^2(s,s')}{\beta_{y0}}\right)+\sigma_\delta^2R_{56}^2(s,s')\end{array}\right]\right\} \quad (10)$$

with

$$\begin{aligned}R_{56}(s'\to s)=&R_{56}(s)-R_{56}(s')+R_{51}(s')R_{52}(s)-R_{51}(s)R_{52}(s')\\&+R_{53}(s')R_{54}(s)-R_{53}(s)R_{54}(s')\end{aligned} \quad (11)$$

and $R_{5i}(s,s')=C(s)R_{5i}(s)-C(s')R_{5i}(s')$ for i = 1, 2, 3, 4, 6.

Here the kernel function $K(s,s')$ describes relevant collective effects, $g_k(s)$ the resultant bunching factor as a function of the longitudinal position given a wavenumber k, and $g_k^{(0)}(s)$ is the bunching factor in the absence of collective effect (i.e. from pure optics effect). We particularly note that the above formulation can be applicable to the case with focusing in combined-function dipoles.

ISBN 978-3-95450-183-0

In the above formulation, we have made the coasting beam approximation, i.e. the modulation wavelength is assumed much shorter compared with the whole bunch duration. The transport functions $R_{5i}(s)$ (i = 1, 2, 3, 4, 6) are adopted from ELEGANT with slight modification to account for "non-ultrarelativistic" contribution $R_{56}(s) \to R_{56}(s) + \frac{s}{\gamma^2}$ where s is the longitudinal coordinate along the beamline. Here we define the microbunching gain function at $k = 2\pi/\lambda$ as $G(s) \equiv \left| g_k(s)/g_k^{(0)}(0) \right|$ and the gain spectral function at the exit of a lattice as

$$G_f(\lambda) \equiv G(s = s_f) \tag{12}$$

We note that the impedance term in Eq. (9) is of our primary interest. With given impedance models [Eqs. (1-7)], we can estimate the microbunching gain through a beamline. Since the calculation is fast (compared with tracking simulation), it can be used to make quick estimation or optimize the microbunching gain development in a lattice design.

For Eq. (8), we solve it by two approaches: one is the *direct* solution, and the other resorts to the *iterative* solution. For the latter approach, at the first step, we express Eq. (8) in vector forms for $g_k(s)$ and $g_k^{(0)}(s)$, and in a matrix form for $K(s,s')$. Then we arrive at the following equation

$$\mathbf{g}_k = \left(\mathbf{I} - \mathbf{K}\right)^{-1} \mathbf{g}_k^{(0)} \tag{13}$$

provided the inverse matrix of $\left(\mathbf{I} - \mathbf{K}\right)$ exists.

At the second step, to introduce the stage gain concept, motivated by Ref. [4], we try to define the first-order iterative solution by expanding Eq. (13) as: $\mathbf{g}_k^{(1)} = \left(\mathbf{I} + \mathbf{K}\right)\mathbf{g}_k^{(0)}$ and the second-order iteration to be $\mathbf{g}_k^{(2)} = \left(\mathbf{I} + \mathbf{K} + \mathbf{K}^2\right)\mathbf{g}_k^{(0)}$. In general, to n^{th} order iterative solution, we have

$$\mathbf{g}_k^{(n)} = \left(\sum_{m=0}^{n} \mathbf{K}^m\right)\mathbf{g}_k^{(0)} \tag{14}$$

It can be seen that, in Eq. (14), the sum to infinite order should give an equivalent result of Eq. (13) [or, Eq. (8)], provided the sum converges. Therefore, these two approaches, Eq. (8) and Eq. (14), can be proven equivalent. Here we note that the convergence of Eq. (14) is held in a single-pass (or, finite-pass) system, e.g. the transport or recirculation arcs, for CSR effects. For a storage ring or for LSC effects which are ubiquitous along the beamline, the convergence would not be held, which is however beyond the scope of this paper [20]. For CSR-induced microbunching gain, the advantage of using numerical iterative approach, Eq. (14), is that it can give us a further insight to see how different orders of iterative solutions contribute to the different physical amplification stages. Also, Eq. (14) facilitates us exploring up to which stage the overall CSR-induced microbunching development can be described, by comparing with the direct solution [1]. Hereafter we dub the solutions of Eq. (13) as *direct* solutions, and those of Eq. (14) as *iterative* solutions. Note that the definition of gain function with respect to Eq. (8) [i.e. Eq. (12)] can now be generalized to define the staged gain function, with respect to Eq. (14), as $\tilde{G}^{(n)}(s) = \mathbf{g}_k^{(n)}(s)/\mathbf{g}_k^{(0)}(0)$ with $G^{(n)}(s) = \left|\tilde{G}^{(n)}(s)\right|$ and, similar to Eq. (12), the stage gain spectral function,

$$G_f^{(n)} \equiv G^{(n)}(s = s_f) \tag{15}$$

To further compare the CSR microbunching gains contributed from individual stages, we devise in this subsection a method to quantitatively characterize the microbunching amplification in terms of stage orders. We note that Eq. (15) can in general be expanded in a series of polynomial of the beam current as [see also Eq. (14) and (9)]

$$\tilde{G}_f^{(M)} = \tilde{G}^{(M)}(s = s_f) = \tilde{G}_0 + \tilde{G}_1 I_b + \ldots + \tilde{G}_M I_b^M = \sum_{m=0}^{M} \tilde{G}_m I_b^m \tag{16}$$

up to a certain order M.

In order to extract the net effects caused by the lattice optics and beam phase space spreads for Landau damping, the above expression Eq. (16), together with knowledge of Eq. (9), can be further formulated as

$$\tilde{G}_f^{(M)} = \sum_{m=0}^{M} A^m d_m^{(\lambda)} \left(\frac{I_b}{\gamma I_A}\right)^m \tag{17}$$

where A is defined in Eq. (2), γ is the relativistic factor and $d_m^{(\lambda)}$ is the dimensionless coefficient (given a certain modulation wavelength) which now reflects the properties from lattice optics at m^{th} stage (m = 0, 1, 2,…), as well as Landau damping through finite beam emittances and energy spread [see Eqs. (10)]. For our interest in the following discussion, λ is chosen to correspond to the maximal CSR gain, denoted as λ_{opt}. Here we point out that Eq. (38) of Ref. [4] can be a special case of Eq. (17) for $M = 2$ in a typical bunch compressor chicane.

Obtaining the coefficients $d_m^{(\lambda)}$ of Eq. (17) can be straightforward. Here we remark the close connection between Eq. (9) and Eqs. (14, 15). For now, we can define the *individual* stage gain, which shall be convenient for our further discussion,

$$\mathcal{G}_f^{(m)} = \left| A^m d_m^{(\lambda)} \left(\frac{I_b}{\gamma I_A}\right)^m \right| \tag{18}$$

Note the difference between Eq. (17) and (18).

As our second model to calculate the microbunching gains, we use ELEGANT [5,6], based on the particle tracking, as our benchmarking against the results by our semi-analytical Vlasov solver for the following example lattices.

SIMULATION RESULTS

High-energy Transport Arcs (Example 1 and 2)

In this section we take two 1.3 GeV high-energy transport arcs as our comparative examples (hereafter dubbed Example 1 and Example 2 lattice). The detailed description of the two example lattices can be found in Ref. [21, 22]. Table 1 summarizes some initial beam

ISBN 978-3-95450-183-0

parameters for use in our simulations. Here, Example 1 lattice is a 180° arc with large momentum compaction (R_{56}), as well as a second-order achromat and being globally isochronous with a large dispersion modulation across the entire arc. In contrast to the first example, Example 2 is again a 180° arc with however small momentum compaction. This arc is also a second-order achromat but designed to be a locally isochronous lattice within superperiods. Local isochronisity ensures that the bunch length is kept the same at phase homologous CSR emission sites. The lattice design strategy was originally aimed for CSR-induced beam emittance suppression, while our simulation results show that it appears to work for microbunching gain suppression as well. Figure 1 shows the Twiss functions and transport functions R_{56}(s) (or, the momentum compaction functions) across the arcs. Note that R_{56}(s) for Example 2 (Fig. 1d) is much smaller in amplitude than that for Example 1 (Fig.1c) due to local isochronicity.

Table 1: Initial Beam and Twiss Parameters for the Two High-energy Transport Arcs

Name	Example 1 (large R_{56})	Example 2 (small R_{56})	Unit
Beam energy	1.3	1.3	GeV
Bunch current	65.5	65.5	A
Normalized emittance	0.3	0.3	μm
Initial beta function	35.81	65.0	m
Initial alpha function	0	0	
Energy spread (uncorrelated)	1.23×10^{-5}	1.23×10^{-5}	

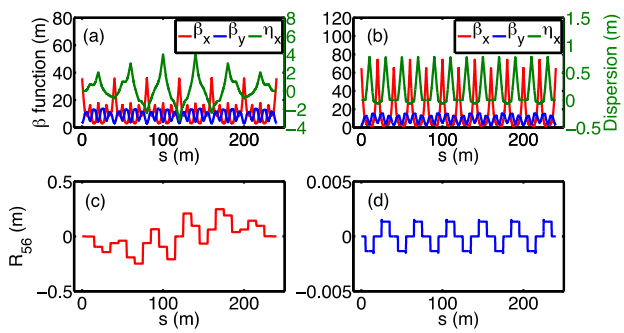

Figure 1: Lattice and transport functions for 1.3 GeV high-energy transport arc: (a)(c) with large momentum compaction function R_{56} (Example 1); (b)(d) with small momentum compaction function R_{56} (Example 2).

Microbunching gains for the two transport arcs are shown in Figs. 2 and 3. Figure 2 shows the gain spectra $G_f(\lambda)$ at the exits of the lattices as a function of modulation wavelength, from which one can obviously see a significant difference between them: Example 1 is vulnerable to CSR effect while Example 2 is still laid a very low level.

One can observe that microbunching gain with the inclusion of both steady-state CSR and entrance transient effects is slightly lowered from the case of steady-state CSR alone. This is because the CSR impedances including entrance transient effect become a bit reduced near a dipole entrance where the beam enters a bend. One can also observe that, with the inclusion of all relevant CSR impedances, including exit transients, the microbunching gain increases up to 200 % compared with that of steady-state case. It can be also expected that the additional inclusion of LSC can further degrade the longitudinal beam quality. Note that, for this lattice (Example 1), all the dipoles only occupy less than 5% of total beamline length, so without optical compensation the CSR-drift transient can cause a further significant effect. Yet with optical compensation, even with the same ratio of dipoles over the beamline, Example 2 is not subject to CSR-induced MBI. This highlights the impact of lattice design for transport or recirculation arcs on microbunching gain. We remind that, due to extremely high gain of Example 1 lattice with inclusion of all relevant CSR impedances, those ELEGANT results are averaged over the initial amplitudes 0.01-0.04% and 70×10^6 macroparticles are used in the simulation with extensive convergence studies done before ELEGANT production [23].

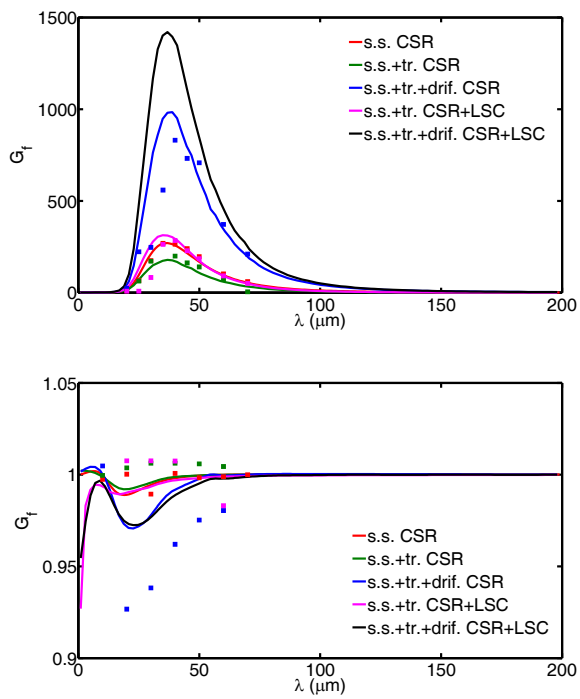

Figure 2: Microbunching gain spectra as a function of initial modulation wavelength for Example 1 (top) and Example 2 (bottom) lattice. Here, for ELEGANT tracking of Example 1, we vary the initial density modulation

ISBN 978-3-95450-183-0

amplitudes from 0.04 % to 0.1 % for various modulation wavelengths in order to obtain the converged results.

Figure 3 demonstrates the evolution of microbunching gains as a function of s for several different combination of impedances at optimal wavelengths (λ_{opt} = 40 μm for Example 1; λ_{opt} = 20 μm for Example 2). One can see in Fig. 3, with inclusion of CSR drift, the gain greatly accumulates at the second half of Example 1, while Example 2 (with local isochronicity) is free from the gain amplification. With further inclusion of LSC, the gain increases more, but primary contribution to the overall gain comes from CSR effect.

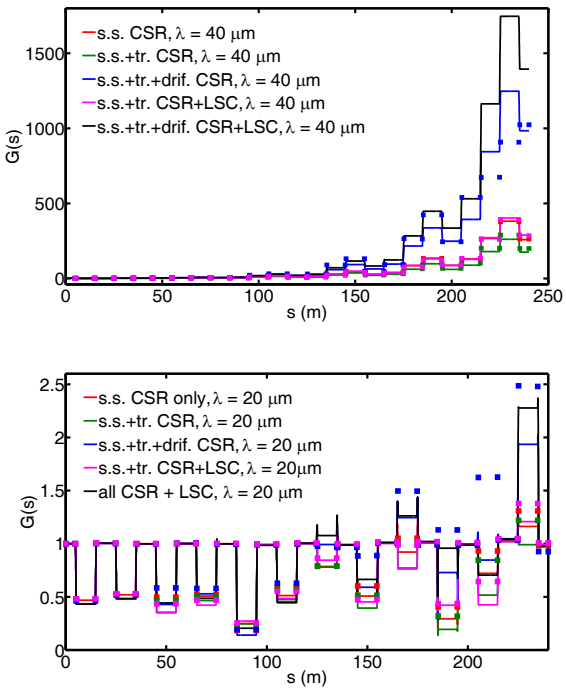

Figure 3: Microbunching gain functions G(s) for Example 1 (top) and Example 2 (bottom) lattice. Note here that we impose an initial density modulation amplitude 0.05 % on a flattop density distribution in ELEGANT simulations for Example 1.

To further examine the features of multi-stage gain amplification, we continue to take the two high-energy transport arcs (Example 1 and 2) as examples to extract the coefficients $d_m^{(\lambda)}$ [defined in Eq. (17)] so that we can quantify and compare optics impacts on the CSR microbunching gains (for simplicity, here we consider only steady-state CSR effect). Provided a set of $d_m^{(\lambda)}$ are given for different stages (i.e. different m), Fig. 4 shows the bar charts representing the individual staged gains $\mathcal{G}_f^{(m)}$ as functions of beam current and stage index for both Examples. Here we have two observations in Fig. 4: first, given a specific stage index, as the beam current increases, $\mathcal{G}_f^{(m)}$ also increases; second, for the same beam current, as the stage order increases, $\mathcal{G}_f^{(m)}$ does not necessarily increase accordingly. This is because the stage gain coefficient's behavior is lattice dependent. Since $d_m^{(\lambda)}$ are independent of beam current and beam energy, they can be used to obtain the maximal gain as a function of the beam current provided $d_m^{(\lambda)}$ are given. Figure 5 compares the overall gain from Eq. (17) and Eq. (12) for different currents for Example 1 and 2, at a selected wavelength close to maximal gain. As can be seen, M = 6 can well describe the current dependence of the CSR microbunching gain in Example 1 lattice. For Example 2 case, the nominal beam current (65.5 A) is well described by M = 6; however, if at further high current scale, it needs to take higher stage orders into account.

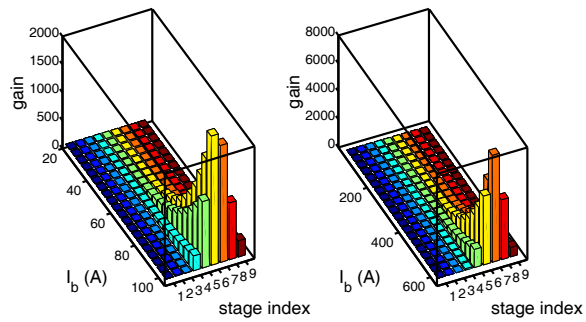

Figure 4: Bar chart representation of the individual staged gains [Eq. (18)] at the exits of the Example 1 and 2 lattices for several different beam currents. (Left) Example 1 (λ = 36.82 μm); (right) Example 2 (λ = 19 μm).

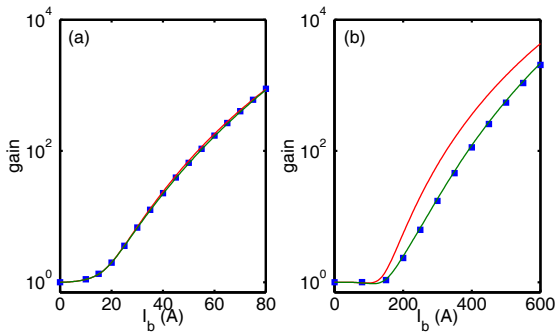

Figure 5: Current dependence of maximal CSR gain for the two high-energy transport arc lattices: (a) Example 1; (b) Example 2. Solid red line from Eq. (12) with M = 6, solid green line from Eq. (12) with M = 9 and blue square dots from Eq. (17).

To further illustrate how the multi-stage amplification physically contributes to and how the lattice optics impacts on the microbunching development, we create in Fig. 6 the "quilt" patterns $R_{56}(s' \to s)$ [defined in Eq. (11)] for the two example lattices in order to clearly identify the enhancement or suppression of

ISBN 978-3-95450-183-0

microbunching along the beamline by lattice optics. For a planar and uncoupled lattice, Eq. (11) is reduced back to $R_{56}(s' \to s) = R_{56}(s) - R_{56}(s') + R_{51}(s')R_{52}(s) - R_{51}(s)R_{52}(s')$. The upper left area in the figures vanishes due to causality. It is obvious that in Example 1 (left figure) those block areas with large amplitude, particularly the bottom right deep red blocks, can potentially accumulate the CSR gain. To be specific, for Example 1, energy modulation at s' = 15 m can cause density modulation at s = 60 m, where CSR can induce further energy modulation at the same location. Then such modulation propagate by $R_{56}(s' \to s)$ from s' = 60 m to s = 100 m, and so on. It is this situation that causes multi-stage CSR amplification. Here we note that more complete analysis needs to take Landau damping factor into account and we refer the interested reader to Ref. [24]. In contrast, the situation for Example 2 (right figure) is more alleviated because of much smaller amplitudes of $R_{56}(s' \to s)$.

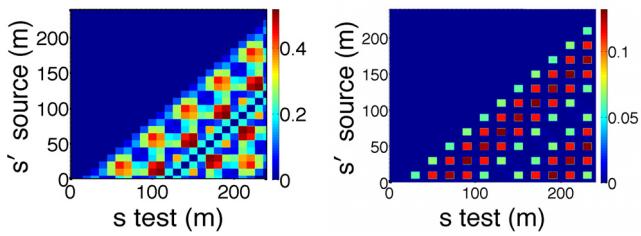

Figure 6: $R_{56}(s' \to s)$ quilt patterns for the two Example lattices: Example 1 (left) and Example 2 (right).

The third example is based on the circulator cooling ring (CCR) for MEIC [7]. Maintaining excellent phase space quality for the electron beam is known crucial to the electron cooling efficiency. This preliminary design is based upon the topological structure of figure-8 collider ring. Such design of an ERL-based electron cooler ring is characteristic of two 30-m cooling solenoids cross the center of the electron collider ring and composed of horizontal dipoles around the four corners and vertical bending dipoles around the two non-diagonal corners to meet the requirement of 3 stacked figure-8 rings [7]. Note here that the transverse beam dynamics in horizontal and vertical planes are coupled in the cooling solenoids, though our theoretical formulation [Eq. (8)] assumes no coupling. Note however that the first-order transfer matrix of a solenoid does not couple the transverse degrees of freedom to the longitudinal motion. Therefore, we remove the solenoid sections out from our simulations without affecting the CSR microbunching dynamics within the framework [25]. Table 2 lists the initial beam and Twiss parameters for MEIC CCR [7].

Table 2: Initial Beam and Twiss Parameters for MEIC CCR [7]

Name	Value	Unit
Beam energy	54	MeV
Beam current	60	A
Normalized emittances	3 (in both planes)	μm
Initial beta functions	10.695/1.867	m
Initial alpha functions	0 (in both planes)	
Energy spread (uncorrelated)	1.0×10^{-4}	

Microbunching gain spectra $G_f(s)$ from Eq. (8) for different combinations of impedance models are demonstrated in Fig. 7 where we found the microbunching gains with $\lambda \approx 350$ μm reach the maximal. Unlike Example 1 and 2, LSC shows a detrimental effect on MEIC CCR, due to (relatively) low beam energy and high bunch charge. Figure 8 shows the gain evolution $G(s)$ along the ring, where we can see the microbunching gain starts to build up at the second arc ("10-o'clock arc"), continually develop at the third arc, and eventually increase to a huge level when the beam is sent back to the beam exchange system.

Our study indicates that the preliminary design of CCR for high-energy electron cooling is at risk of microbunching instability; an improved design is required to suppress such instability and/or alternative beam transport scheme would be considered in order to compensate and to circulate the electron beam as many turns as possible [7] while maintaining high phase space quality of the electron beam required by sufficient electron cooling efficiency.

We emphasize here that, for MEIC CCR, due to its high bunch charge (~ 2 nC) as well as low energy spread (~ 10^{-4}), as expected, microbunching, greatly accumulates along the beamline and over a broad spectral range of density modulation.

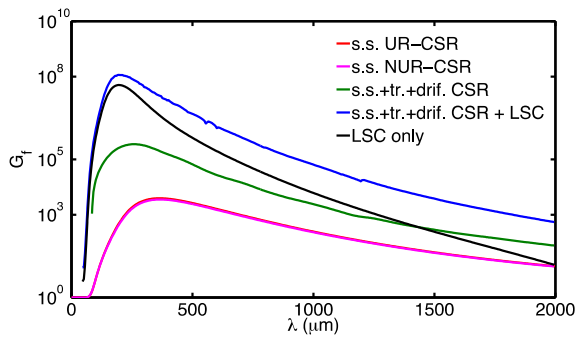

Figure 7: Microbunching gain spectra as a function of initial modulation wavelength for MEIC CCR lattice. Note that, due to ultrahigh gain, we do not benchmark these results directly, but we do for a case with 10 times larger the transverse emittances and have confirms the validity of our simulation results [24].

ISBN 978-3-95450-183-0

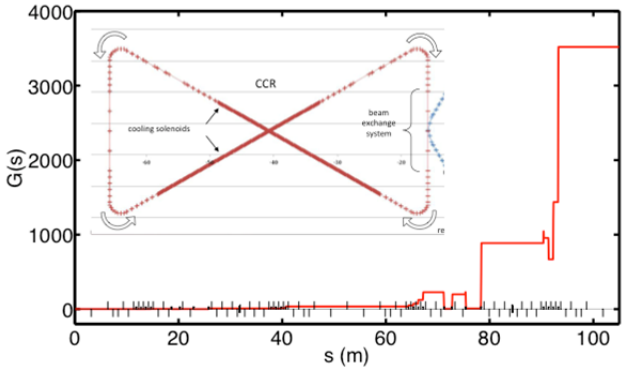

Figure 8: Microbunching gain functions G(s) for MEIC CCR lattice; here λ = 350 μm. The inset illustrates schematic layout of the circulator ring.

SUMMARY AND CONCLUSION

In this paper, we have first summarized relevant impedance models for microbunching instability study, including CSR and LSC, and outlined the theoretical formulation based on (linearized) Vlasov equation by treating this problem in frequency domain. The solution to the governing equation [Eq. (8)] can be self-consistently obtained (i.e. direct solution) or found through numerical iteration (i.e. iterative solution). With introduction of stage gain concept, the individual iterative solutions can be connected through the lattice optics $R_{56}(s' \to s)$ in a physical way. Moreover, the stage gain coefficient [defined in Eq. (17)] can be applied to make quick estimation for the maximal CSR gain provided a lattice is given (Fig. 5).

Then, we have illustrated, based on two comparative high-energy transport arcs, the optics impact on the microbunching gain development using the developed stage gain concept. We also presented the microbunching gain analysis for a circulator cooling ring design of MEIC and concluded that such preliminary design is subject to both CSR and (primary) LSC induced microbunching instability.

Finally, it is interesting that although the emittance preservation is of original/primary consideration for the proposed Example 2 design [21, 22], it also works well for microbunching gain suppression.

ACKNOWLEDGMENT

The author (C. -Y. T.) would like to express his sincere thanks to his advisors, Mark Pitt and Rui Li for their kind support and many fruitful discussions. We also thank Steve Benson for bringing many motivating issues for our studies. This work is supported by Jefferson Science Associates, LLC under U.S. DOE Contract No. DE-AC05-06OR23177.

REFERENCES

[1] C. -Y. Tsai et al., Theoretical investigation of coherent synchrotron radiation induced microbunching instability in transport and recirculation arcs, International FEL Conference 2014 (THP022)

[2] C. -Y. Tsai et al., CSR induced microbunching gain estimation including transient effects in transport and recirculation arcs, IPAC'15 (MOPMA025)

[3] S. Heifets et al., Coherent synchrotron radiation instability in a bunch compressor, Phys. Rev. ST Accel. Beams 5, 064401 (2002) and its erratum paper

[4] Z. Huang and K. -J. Kim, Formulas for coherent synchrotron radiation microbunching in a bunch compressor chicane, Phys. Rev. ST Accel. Beams 5, 074401 (2002) and its erratum paper

[5] M. Borland, elegant: A Flexible SDDS-Compliant Program for Accelerator Simulation, APS Light Source Note LS-287, September 2000

[6] M. Borland, Modeling of microbunching instability, Phys. Rev. ST Accel Beams 11, 030701 (2008)

[7] MEIC Design Summary, available at http://arxiv.org/abs/1504.07961

[8] Y. Roblin et al, Experimental studies of optics schemes at CEBAF for suppression of coherent synchrotron radiation (CSR), JLab LDRD (2014)

[9] R. Li et al., Experimental investigation of LSC and CSR induced microbunching instability using LERF, JLab LDRD, submitted (2015)

[10] R. Li and C. -Y. Tsai, CSR impedance for non-ultrarelativistic beams, IPAC'15 (MOPMN004)

[11] J. Murphy et al., Longitudinal wakefield for an electron moving on a circular orbit, Part. Accel. 1997, Vol. 57, pp. 9-64

[12] Ya. S. Derbenev et al., Microbunch radiative tailhead interaction, TESLA-FEL-Report 1995-05

[13] D. Zhou, An alternative 1D model for CSR with chamber shielding, IPAC'12 (MOOBB03)

[14] C. Mitchell et al., Effects of transient CSR wakefields on microbunching in a bunch compressor, IPAC'13 (TUPWA057)

[15] E. L. Saldin et al., On the coherent radiation of an electron bunch moving in an arc of a circle, NIMA 398, 373 (1997)

[16] R. Bosch et al., Longitudinal wake of a bunch of suddenly accelerated electrons within the radiation formation zone, Phys. Rev. ST Accel. Beams 10, 050701 (2007)

[17] M. Venturini, Models for longitudinal space charge impedance for microbunching instability, Phys. Rev. ST Accel. Beams 11, 034401 (2008)

[18] J. Wu et al., Analytical Analysis of longitudinal space charge effects for a bunched beam with radial dependence, Phys. Rev. ST Accel. Beams 11, 040701 (2008)

[19] M. Venturini et al., Dynamics of longitudinal phase-space modulation in an RF compressor for electron beams, Phys. Rev. ST Accel. Beams 13, 080703 (2010)

ISBN 978-3-95450-183-0

[20] R. Warnock, private communication (2014)
[21] D. R. Douglas et al., Control of coherent synchrotron radiation and microbunching effects during transport of high brightness electron beams, arXiv: 1403.2318v1 [physics.acc-ph]
[22] D. R. Douglas et al., Control of synchrotron radiation effects during recirculation, IPAC'15 (TUPMA038)
[23] C.-Y. Tsai and R. Li, Simulation of coherent synchrotron radiation induced microbunching gain using ELEGANT, JLAB-TN-14-016
[24] C. -Y. Tsai et al., (to be published)
[25] Numerical tracking simulation confirms that such artificial removal of solenoid sections does not affect CSR-induced microbunching gains; however, we believe LSC can have an additional effect due to such long cooling sections.

ISBN 978-3-95450-183-0